

GPR data interpretation using continuous wavelet transform: a different approach

Sarvesh Kumar*, Sanjit Kumar Pal, Soma Rani and Saurabh

Department of Applied Geophysics, Indian Institute of Technology (Indian School of Mines), Dhanbad 826 004, India

The objective of this communication is to establish a new technique for GPR data interpretation using continuous wavelet transform (CWT) approach. In the present study, we have adapted the CWT technique to detect the edges or abrupt changes in the signal. For validation of the proposed technique, we have acquired data over a known tunnel in point mode and time mode using two antennas of two different frequencies (40 MHz and 80 MHz). The tunnel is already known in the area, however information of overburden depth and extension of the tunnel was not properly known. Initially, GPR data have been processed using standard processing (RADAN 7.0) software and the tunnel has been delineated by the two small peaks in the signal. Sometimes, it becomes tough to interpret the small changes or discontinuities in the reflected GPR signal processed by the available standard software. Further, CWT has been performed on a wavelet around the same time depth at which tunnel has been detected based on the standard processing of the GPR data. The tunnel has been prominently delineated by the high wavelet coefficient values. A comparative analysis for width and depth estimation using GPR data and CWT technique has been carried out. While implementing CWT, it is essential to choose the suitable mother wavelet for high-resolution scalogram plot. Mother wavelet for our study area has been selected based on the maximum normalized mean power value of wavelet coefficients. We discuss an approach for tunnel detection and provide an efficient procedure to improve detection performance.

Keywords: CWT, dielectric, GPR, mother wavelet, scalogram, tunnel.

NOWADAYS, ground penetrating radar (GPR) is the most extensively used geophysical technique by different community mainly, civil engineers and geotechnical engineers, for quick and high-resolution imaging of the shallow surface. This geophysical method is generally used to extract subsurface information based on the dielectric contrast of the medium. GPR works on the principle of transmission, reflection and receiving of an electromagnetic (EM) wave of high frequency (10 MHz–2.5 GHz) normal to the ground surface. GPR has many applications in geological profiling¹, pipe and cable

detection², archaeology^{3,4}, tunnelling^{5–7} and coal bed thickness detection^{8,9}. Under promising conditions, GPR can provide detailed information very rapidly and efficiently regarding the nature of buried objects¹⁰. The EM wave is reflected from a boundary or buried object with different dielectric constants to the surface at the receiving antenna to record the variations in the reflected signal. The GPR principle is similar to reflection seismology, except that EM wave is used instead of an acoustic signal, and reflections appear at boundaries with prominent contrast of dielectric constant instead of impedance contrast. In tunnel detection, EM pulses may be attenuated due to dispersion and formation conductivity, which generates noise in the signal¹¹. The attenuation of EM pulses may also increase owing to rise in dielectric permittivity, which mainly occurs due to upsurge in the moisture content of the material.

In the GPR signal, identification of small-scale discontinuity is difficult and most of the time creates ambiguities during interpretation. GPR uses very high frequency signal for data acquisition and thus, gives high-resolution shallow surface information. At shallower depth, there may be various objects which reflect the GPR signal and create confusion with the main object. Also, one of the common problems encountered in GPR data acquisition is interference of noise in the signal, which may mask the reflected signal. To encounter these problems we generally use different filtering techniques for processing of GPR data. To enhance the features detected in the GPR survey, it is important to remove noise without losing the main signal. The continuous wavelet transform (CWT) technique has been found to be the suitable approach to resolve these problems^{12–14}. In this communication, we have attempted a new approach for analysing GPR signals using CWT. Wavelet transform technique is well established method for analysis of well-logging^{15,16}, gravity¹⁷ and magnetic data¹⁸. In the present study, we have adapted this technique for analysis of GPR data. Chandrasekhar and Rao¹⁵ implemented wavelet analysis on well-log data to determine the space-localization of the oil and/or gas formation zones. Mukherjee *et al.*¹⁶ employed wavelet and Fourier transforms on well log data for the identification of formation interfaces. There are very few studies based on uses of wavelet transform for interface or discontinuity detection in GPR data. Quadfeul and Aliouane¹⁹ used the wavelet transform technique for noise attenuation from GPR data using wavelet transform and artificial neural network (ANN). Liu and Oristaglio²⁰ carried out a study for parameter estimation using the wavelet transform. This communication discusses a combined approach of conventional and CWT techniques on GPR data for the better understanding of small-scale discontinuity in the subsurface. For a case study, a known tunnel has been selected, however information of overburden depth and extension of the tunnel was not properly known.

*For correspondence. (e-mail: jhasarvesh90@gmail.com)

The high frequency EM wave generated using antenna propagates inside the earth with different permittivity value depending on the water content, dissolved minerals and clay content²¹⁻²⁴. The wave gets reflected to the surface from a layer having different dielectric properties from the surrounding medium. The reflected signal is detected by the receiving antenna at the surface. The reflected wave received by a receiver antenna at the surface is stated as scan and recorded on a digital storage device for later interpretation. The propagation velocity of EM waves does not change in a specific medium, so for reflection wave total travel time (ΔT) is used to estimate the depth (D) of the geological interface with different permittivity value and it can be written as²⁵

$$D = VX\Delta T/2, \tag{1}$$

where V is the propagation velocity of EM waves in the media and depends primarily on the permittivity of the material. It can be written as²⁵

$$V = C/\sqrt{\epsilon}, \tag{2}$$

where C is the propagation velocity (3×10^8 m/s) of electromagnetic waves in the atmosphere and ϵ is the relative permittivity of the medium. The depth of penetration depends mainly on antenna frequency, dielectric properties (relative permittivity) of subsurface and moisture content. Antennas convert electric currents into electromagnetic waves that propagate into a material just like a transducer. The amplitude of the reflected GPR signal is proportional to the reflection coefficient. The reflection coefficient R can be represented as²⁶

$$R = \frac{\sqrt{\epsilon_1} - \sqrt{\epsilon_2}}{\sqrt{\epsilon_1} + \sqrt{\epsilon_2}}. \tag{3}$$

The intensity of the reflected signal depends on the contrast of relative dielectric constant between the adjacent layers/medium. In general, greater contrast leads to stronger reflected signal.

The continuous wavelet transform constructs a time-frequency illustration of a signal that gives time and frequency localization of a signal. The CWT is the convolution of signal $f(t)$ with time-shifted (τ) and a scaled (s) version of the mother wavelet $\varphi(t)$. The scale of the wavelet means the stretching and shrinking (analogues to frequency) of wavelet, smaller-scale factor results in more compressed wavelet. The frequency range for each scale component can be assigned for different wavelets^{27,28}. In mathematical form CWT can be written as

$$C(\tau, s) \int_{-\infty}^{\infty} f(t) \frac{1}{\sqrt{s}} \varphi^* \left\{ \frac{t-\tau}{s} \right\} dt, \tag{4}$$

where (*) indicates the complex conjugate. The outputs of the CWT are coefficient values, which are estimated at each s by continuously varying τ . The larger value of the CWT coefficient corresponds to the greater resemblance between the shapes of the signal and the wavelet at τ and s , which guide to select the most precise mother wavelet for analysing the signal. The positioning of maxima of the modulus of the CWT at scale s equivalent to the depth level, using this concept depth can be calculated^{29,30}. There are different types of mother wavelets with different properties for specific purposes³¹. It is important to select the suitable mother wavelet to identify the discontinuity and prominent edge effect in GPR data. In this study, we have selected mother wavelet based on the maximum normalized mean power of CWT coefficient values.

In this study, Haar, Gauss and Daubechies mother wavelets have been used. Haar wavelet ($\varphi(t)$) (Figure 1 a) is the oldest, simplest and compactly supported wavelet. It is a sequence of rectangular function (not continuous) at time t , which can be written as

$$\varphi(t) = \begin{cases} 1 & 0 \leq t < 1/2 \\ -1 & 1/2 \leq t < 1. \\ 0 & \text{otherwise} \end{cases} \tag{5}$$

Gauss wavelet ($f(t)$) (Figure 1 b) is the result of derivative of Gaussian probability density function at time t and it is complex valued. It provides phase information and by taking the p th derivative of f it can be written as

$$f(t) = C_p e^{-it} e^{-t^2}, \tag{6}$$

where C_p is the normalization constant.

Daubechies wavelet (db) (Figure 1 c) is compactly supported wavelet because of its finite numbers of non-zero scaling coefficients. The associated scaling filters with Daubechies mother wavelet are minimum phase filters. These wavelets have no explicit expression except for Daubechies wavelet at first level (db1), which is a Haar wavelet.

In the present study, we have used the bistatic mode of the transmitter–receiver (T–R) antennas for the GPR unit to provide high resolving power for interface detection. GPR data have been acquired on the road for 50 m profile length crossing a tunnel normally. Two antennas of frequency 40 MHz and 80 MHz have been used for this survey to provide a suitable bandwidth and beam pattern. The system typically acquires 1024 samples with a 16-bit sampling resolution. We have used bistatic fixed T/R offset (1 m) in continuous mode (time mode) and in static stacking (point mode) mode for both the antennas. The transmitting and receiving antennas are fixed at a separation of 1 m for this survey. The antennas are moved

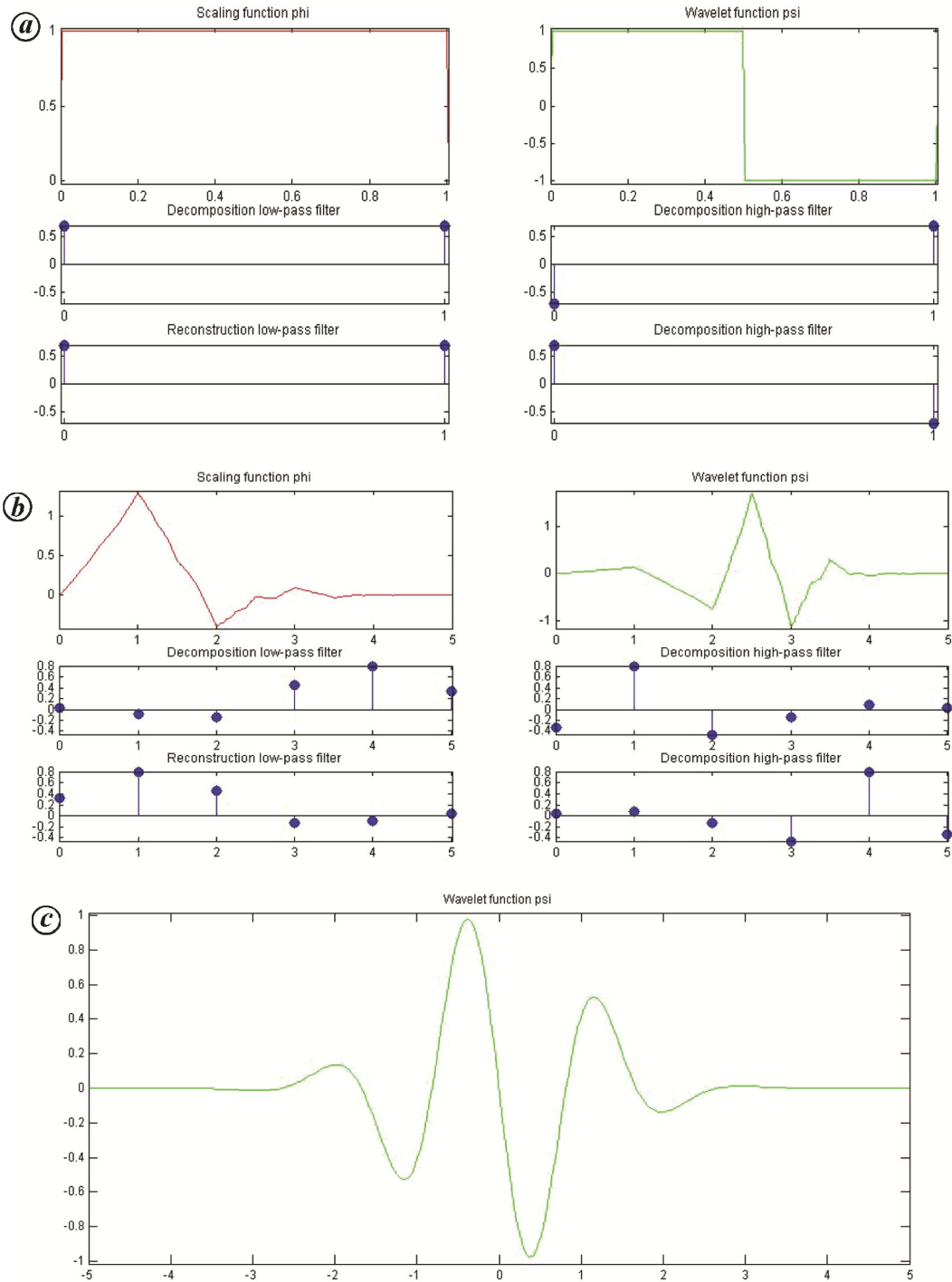


Figure 1. Mother wavelet selected for CWT of GPR signal. *a*, Haar wavelet and its decomposition high pass filter; *b*, Daubechies wavelet at decomposition level 3; *c*, Gauss wavelet at decomposition level 7.

simultaneously over the interested area for scanning in continuous mode.

Whereas in point mode, the antenna set up is the same as the continuous profiling mode. But instead of continuously acquiring data, the antenna system is operated in point-collection mode and the antenna system is moved along a survey line at a fixed interval. Point mode indi-

cates that the data have been collected at different points along a profile with a constant spacing. In the present study, we moved T-R antenna system at each 20 cm distance, i.e. 5 scans (5 data points) in 1 m distance. The scans are collected with the suitable number of stacking (64 stack) to achieve the optimum signal-to-noise.

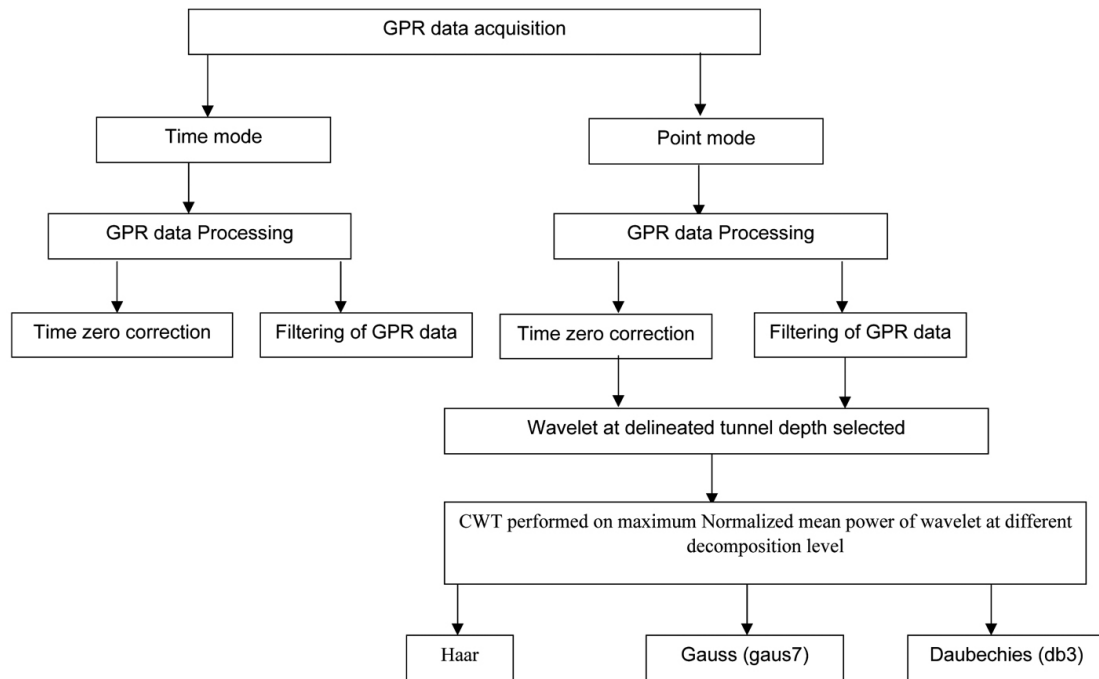


Figure 2. Overall methodology on GPR data processing and application of CWT.

Overall methodology mainly focuses on GPR data processing and application of CWT technique (Figure 2). At the end, an attempt has been made for the conjugate analysis of conventional GPR data interpretation and understanding of GPR output using CWT technique. Initially, point mode and time mode GPR data have been processed using standard processing steps. The time zero correction has been applied to adjust signal position that arises due to the gap between antenna and subsurface. A boxcar filtering has been applied to enhance the signal by removing different types of noise embedded in the signal. After applying all the required processing steps, overburden depth, width and position of the tunnel have been detected.

Further, a wavelet has been picked around the same time depth for CWT analysis. We have used different mother wavelets like Haar, Gauss and Daubechies at different decomposition levels. Mother wavelets at each decomposition level respond differently for the same GPR scan. To overcome this problem, CWT has been applied on each decomposition level and further mother wavelet selected based on the maximum normalized mean power value of wavelet coefficients. The result of CWT on GPR data has been shown only for maximum normalized mean power value of wavelet coefficients for each mother wavelet.

Initially, the continuous mode survey has been carried out to get a close idea about the location of the tunnel. In continuous mode (Figure 3a), it is difficult to calculate the width, overburden depth and the position of the tunnel,

because time-based data has no real distance tag due to uncontrolled manual speed of the antenna system during data acquisition. So it has poor understanding on distance covered at any instantaneous time. However, two edges E1 and E2 can be observed in the profile, which delineate the tunnel. In continuous mode (Figure 3a), GPR signature is not very clear because, it is important to move antenna at a constant speed (some times it is poorly controlled during manual data acquisition), which is a function of the scan spacing (horizontal resolution) of time-based data profiles. Based on continuous mode survey, we have carried out GPR data acquisition in point mode to locate the exact position and overburden depth of the tunnel.

Figure 3b shows the GPR response over the tunnel using 80 MHz antenna in point mode. The tunnel width and overburden depth have been calculated approximately 10 m and 2 m respectively, two edges (kink in the profile) have been observed in each profile, one at 32 m (E3) and another at 42 m (E4) approximately. Figure 3c shows GPR response over the tunnel using 40 MHz antenna in point mode. The edges of tunnel (E5 and E6) have been detected at the same profile distance, width and overburden depth are 10 m and 2 m respectively, results are almost the same as in 80 MHz antenna in point mode. The rectangular blocks R1, R2 and R3 in Figure 3a–c show the ringing noise. These noises arise due to the reverberation of GPR reflected wave^{32,33}. This patch of ringing noise is caused by the void space of the tunnel in both time (R1) and point mode (R2 and R3) GPR data. It

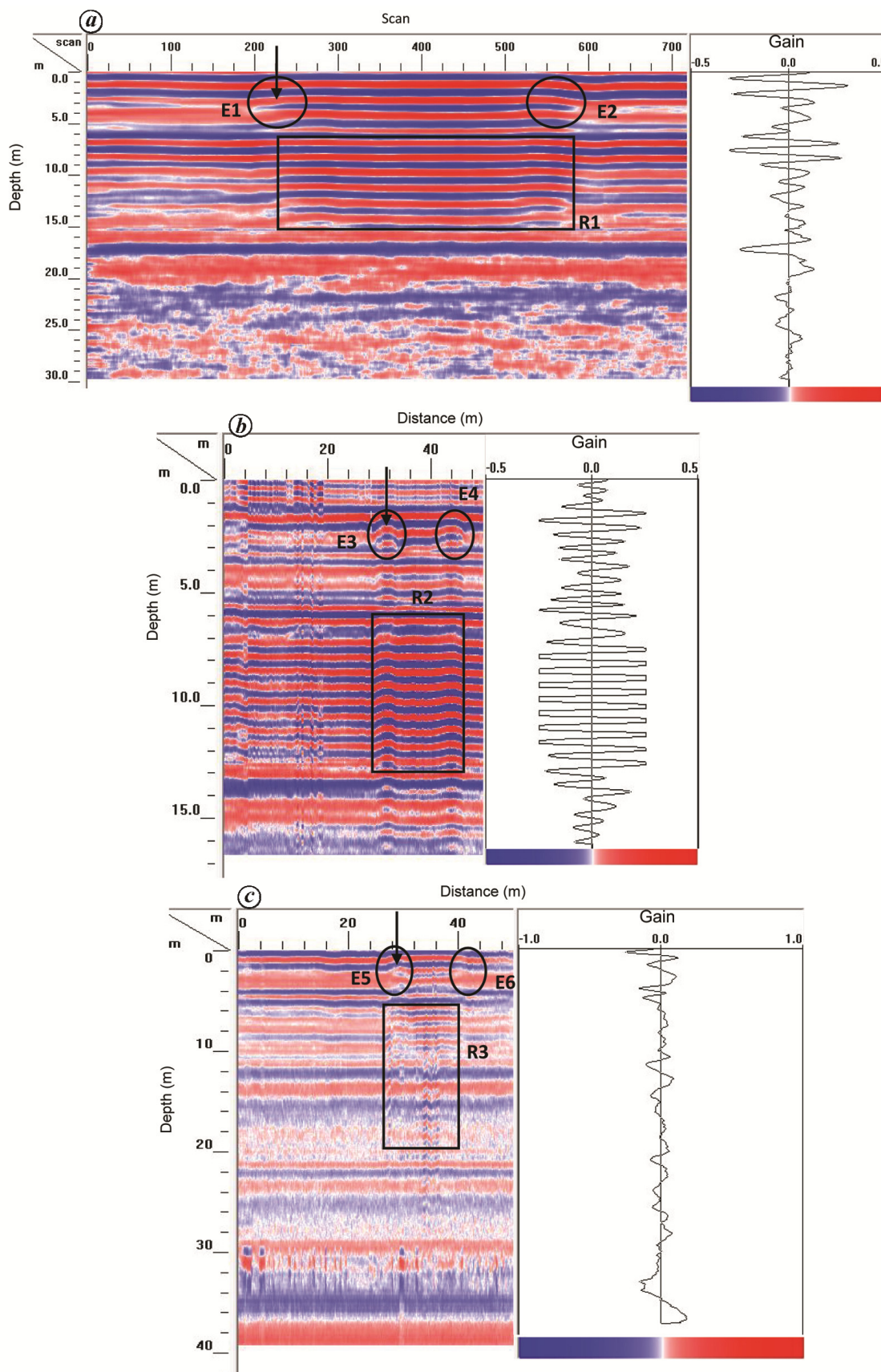


Figure 3. Processed ground penetrating radar section over tunnel. *a*, Time mode section; *b*, 80 MHz point mode section; *c*, 40 MHz point mode section. Vertical down arrow indicates the position of single wave shown in oscilloscope format.

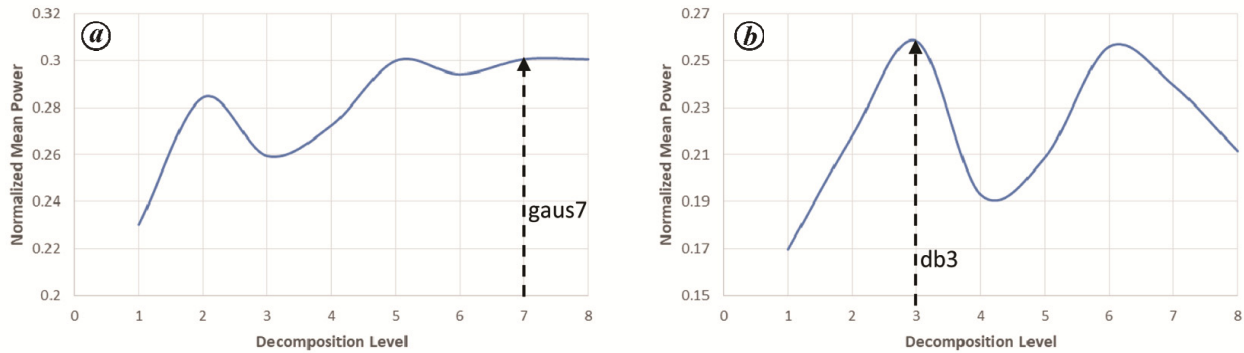


Figure 4. Normalized mean power at different decomposition level. *a*, Gauss (gaus7) mother wavelet; *b*, Daubechies (db3) mother wavelet. Vertical dotted arrow indicates the decomposition level at which Gauss and Daubechies mother wavelet have maximum normalized mean power.

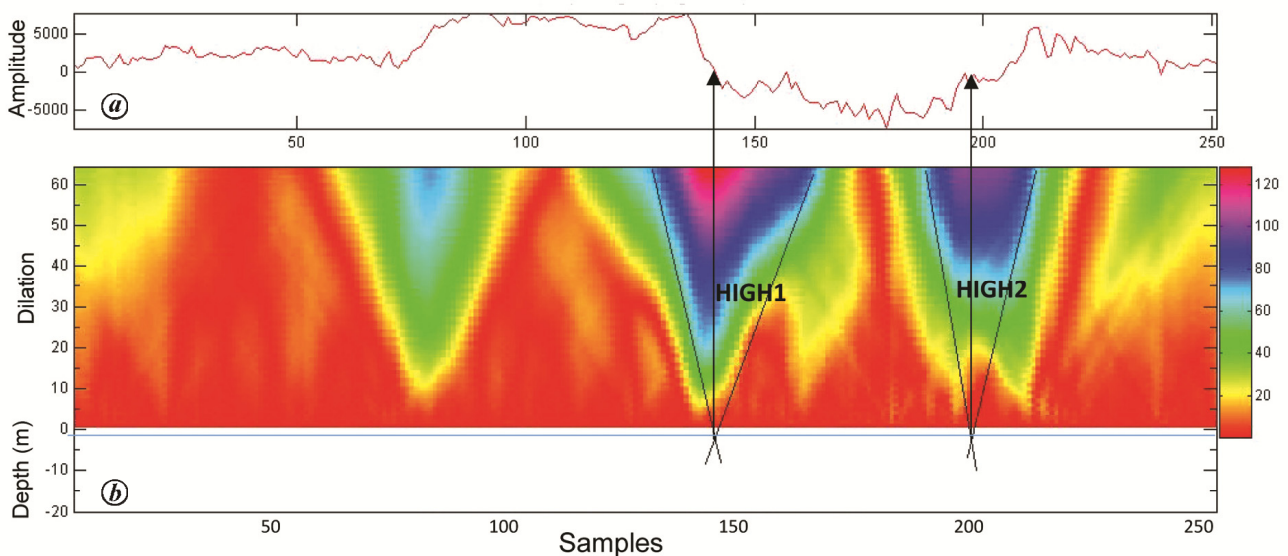


Figure 5. Continuous wavelet transform outputs. *a*, Processed GPR signal; *b*, Scalogram plot using Haar mother wavelet.

can be observed that 40 MHz configuration renders greater depth of penetration but at the expense of vertical resolution (Figure 3 *c*), in comparison to the 80 MHz configuration (Figure 3 *b*).

Further based on GPR data interpretation, we have picked a horizontal wavelet of around the same time depth at which tunnel has been detected. CWT has been performed on the selected GPR wavelet using different mother wavelets. Figure 4 *a* and *b* shows the plot of the normalized mean power of the Gauss and Daubechies mother wavelets. From these plots it can be inferred that maximum normalized mean power of CWT coefficients is associated with Gauss mother wavelet at decomposition level 7 and with Daubechies mother wavelet at decomposition level 3 (db3). Figures 5–7 indicate the continuous wavelet transform coefficient plots for Harr, Gauss (gaus7) and Daubechies (db3) mother wavelets of GPR signal respectively. The abrupt change in GPR signal amplitude can be observed at the maximum value of

the CWT coefficient scale. Figures 5 *a*, 6 *a* and 7 *a* are the GPR signal, which has been selected for CWT analysis. Scalogram plot for Haar (Figure 5 *b*), Gauss7 (Figure 6 *b*) and db3 (Figure 7 *b*) resulted in the high coefficient values (HIGH1 and HIGH2) at the positions where abrupt changes in signal are taking place. The depth has been estimated using CWT technique for all mother wavelet at the maximum dilation value. The depth level is equivalent to the dilation scale (s), which results into the approximately same overburden depth value (~ 2 m) for all mother wavelet. Total number of scans collected for the profile is 250 and in each 1 m distance there are 5 scans (scan/unit is 5). The width of the tunnel has been calculated by subtracting both scan values and then division by 5. Harr mother wavelet (Figure 5 *b*) indicates tunnel boundaries approximately at 140 and 195 scan numbers (i.e. tunnel width ~ 11 m). Similarly, Gauss mother wavelet (Figure 6 *b*) indicates tunnel boundaries approximately at 145 and 195 scan numbers (i.e. tunnel

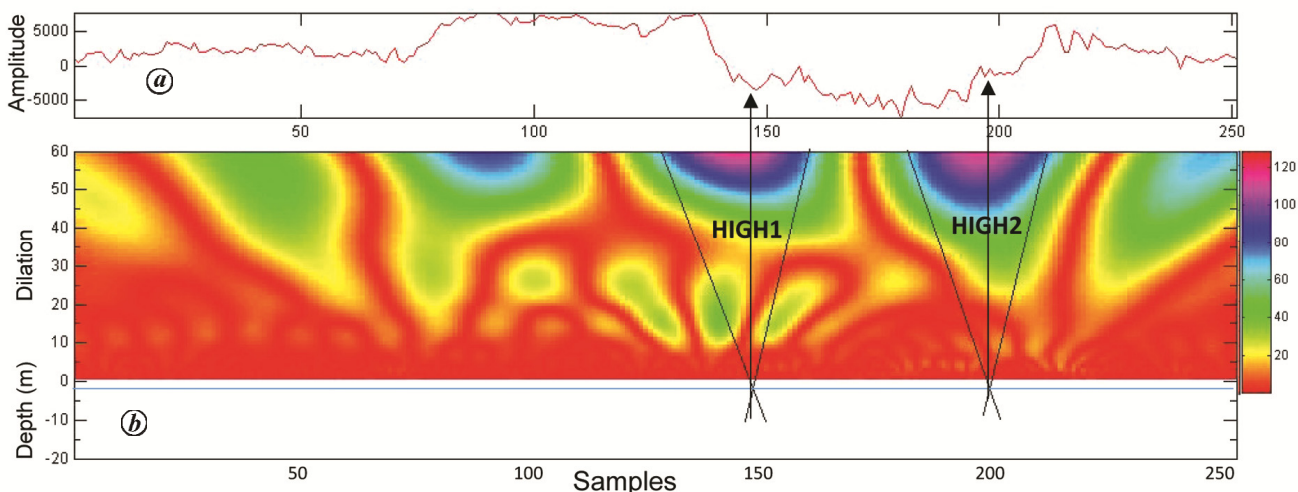


Figure 6. Continuous wavelet transform outputs. *a*, Processed GPR signal; *b*, Scalogram plot using Gauss mother wavelet.

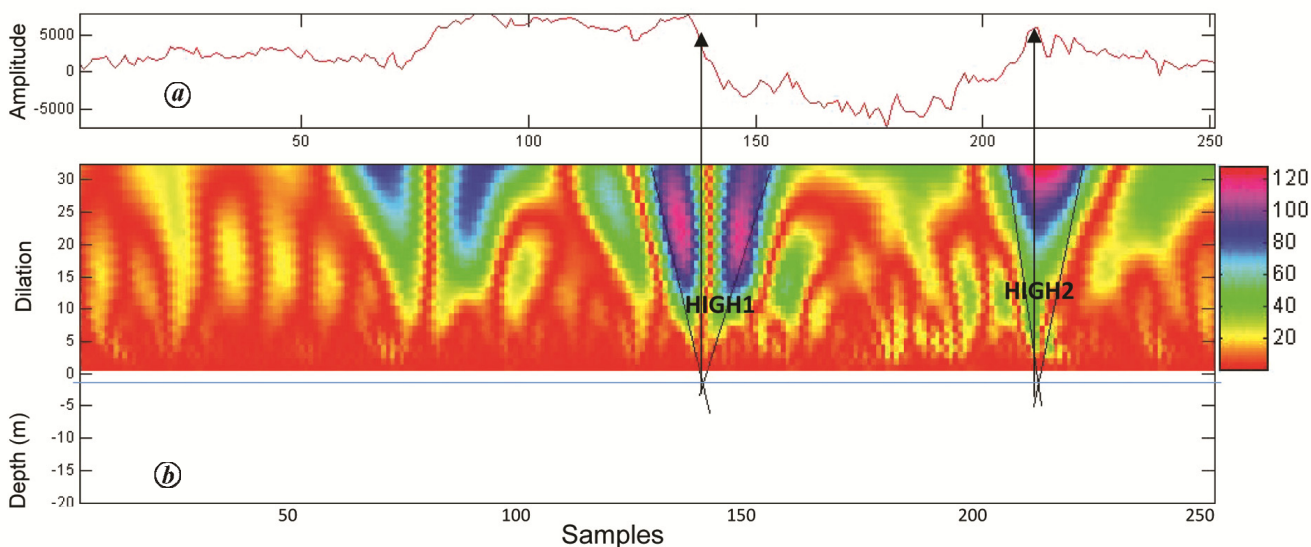


Figure 7. Continuous wavelet transform outputs. *a*, Processed GPR signal; *b*, Scalogram plot using Daubechies mother wavelet.

width ~10 m). Whereas, Daubechies mother wavelet (Figure 7 *b*) indicates tunnel boundaries approximately at 138 and 212 scan numbers (i.e. tunnel width ~15 m).

Initially, we acquired GPR data in time mode over a known tunnel and identified the position of the tunnel after completing the required processing in a standard software. It is observed that time mode data can be used as an initial survey to decide the profile lines for point mode GPR data collection. It is found that depth of penetration of 40 MHz frequency antenna is more than the 80 MHz antenna but at the cost of vertical resolution. CWT technique has been verified as an efficient alternative approach for GPR data interpretation for tunnel detection. A comparative analysis for width and depth estimation using GPR and CWT techniques shows a good

match. Selection of suitable mother wavelet is essential for performing CWT and hence we have selected a mother wavelet with a high value of normalized mean power. In the present study, we have chosen three mother wavelets Haar, Gauss and Daubechies at different decomposition levels. The normalized mean power of wavelet coefficient for Gauss and Daubechies mother wavelets shows the highest value at level 7 (gaus7) and level 3 (db3) respectively, which are further used for CWT. It is observed that CWT using all three mother wavelets indicates the same overburden depth of tunnel, which is approximately 2 m. However, width of the tunnel varies for all mother wavelets. Interestingly, both Harr and Gauss mother wavelets indicate a good match with the results (~10 m width) of the standard software (RADAN) in

delineation of tunnel width. CWT has been found to be an effective alternative approach to interpret the GPR data.

1. Delwar, H., Evaluation of ground penetrating radar and resistivity profilings for characterizing lithology and moisture content changes: a case study of the high-conductivity United Kingdom Triassic sandstones. *J. Geophys. Eng.*, 2013, **10**, 9.
2. Huo, Ni. S., Huang, Y. H., Lo, K. F. and Lin, D. C., Buried pipe detection by ground penetrating radar using the discrete wavelet transform. *Comput. Geotechnol.*, 2010, **37**, 440–448.
3. Shi, Z., Tian, G., Hobbs, R. W., Wo, H., Lin, J., Wu, L. and Liu, H., Magnetic gradient and ground penetrating radar prospecting of buried earthen archaeological remains at the Qocho City site in Turpan, China. *Near Surf. Geophys.*, 2015, **13**, 1–8.
4. Conyers, L. B., *Ground-Penetrating Radar: An Introduction for Archaeologists*, AltaMira Press, Walnut Creek, CA, 1997.
5. Zhao, Y., Wu, J., Xie, X., Chen, J. and Ge, S., Multiple suppression in GPR image for testing back-filled grouting within shield tunnel. In 13th International Conference on Ground Penetrating Radar, Lecce, Italy, 2010.
6. Zhao, Y., Chen, J. and Ge, S., Maxwell curl equation dating for GPR test of tunnel grouting based on Kirchhoff integral solution. In 6th International Workshop on Advanced Ground Penetrating Radar (IWAGPR), Aachen, Germany, 2011, pp. 1–6.
7. Rong, L. X., Xun, S. J., Feng, L. Y., Hong, Z. C. and Yang, X. H., Study on the compound detection method of tunnel cavity disasters. *J. Mining Safety Eng.*, 2011, **4**, 633–637.
8. Ralston, J. and Hainsworth, D. W., Application of ground penetrating radar for coal depth measurement. In IEEE International Conference on Acoustics, Speech and Signal Processing (ICASSP99), 1999, **4**, 2275–2278.
9. Singh, K. K. K., MineVue radar for delineation of coal barrier thickness in underground coal mines: case studies. *J. Geol. Soc. India*, 2015, **82**, 247–253.
10. Singh, K. K. K., Application of ground penetrating radar for hydro-geological study. *J. Sci. Ind. Res.*, 2006, **65**, 160–164.
11. Kuloglu, M. and Chen, C., Ground penetrating radar for tunnel detection. In Geoscience and Remote Sensing Symposium (IGARSS), IEEE International, 2010.
12. Lee, K., Szerbiak, R., McMechan, G. A. and Hwang, N., A 3-D ground-penetrating radar and wavelet transform analysis of the morphology of shore face deposits in the Upper Cretaceous Ferron Sandstone Member, Utah. *AAPG Bull.*, 1996, **93**, 181–201.
13. Zhou, W., Wang, G., Chen, X., Chen, M. and Tian, M., Classification of ground penetrating radar echo signals using wavelet packet and RBF, IEEE Conf Radar, 2006.
14. Idi, B. Y. and Kamarudin, M. N., Interpretation of ground penetrating radar image using digital wavelet transform. *Asian J. Appl. Sci.*, 2012, **5**, 174–182.
15. Chandrasekhar, E. and Rao, V. E., Wavelet analysis of geophysical well-log data of Bombay Offshore Basin, India. *Math Geosci.*, 2012, **44**, 901–928.
16. Mukherjee, B., Srivardhan, V. and Roy, P. N. S., Identification of formation interfaces by using wavelet and Fourier transforms. *J. Appl. Geophys.*, 2016, **128**, 140–149.
17. Singh, A. and Singh, U. K., Wavelet analysis of residual gravity anomaly profiles: Modeling of Jharia Coal Basin, India. *J. Geol. Soc. India*, 2016, **86**(6), 679–686.
18. Goyal, P. and Tiwari, V. M., Application of the continuous wavelet transform of gravity and magnetic data to estimate sub-basalt sediment thickness. *Geophys. Prospect.*, 2014, **62**, 148–157.
19. Ouadfeul, S. A. and Aliouane, L., Noise attenuation from GPR data using wavelet transform and artificial neural network. *Int. J. Appl. Phys. Math.*, 2014, **4**(6), 426–433.
20. Liu, L. and Oristaglio, M., GPR signal analysis: Instantaneous parameter estimation using the wavelet transform. Proceedings of the 7th International Conference on Ground Penetrating Radar, 1998.
21. Topp, G. C., Davis, J. L. and Annan, A. P., Electromagnetic determination of soil water content: measurements in coaxial transmission lines. *Water Resour. Res.*, 1980, **16**, 574–582.
22. Olhoeft, G. R., Applications and limitations of ground penetrating radar. *Soc. Explor. Geophys.*, 1984, 54th Annual International Meeting, Atlanta, GA, pp. 147–148 (abstr.).
23. Haeni, F. P., McKeegan, D. K. and Capron, D. R., Ground penetrating radar study of the thickness and extent of sediments beneath Silver Lake, Berlin and Meriden, Connecticut. *US Geol. Surv. Water Resour. Invest.*, 1987, **19**, 85–4108.
24. Beres, M. and Haeni, F. P., Application of ground-penetrating radar methods to hydrogeologic studies. *Ground Water*, 1991, **29**, 375–386.
25. Benson, A. K., Application of ground-penetrating radar in assessing some geological hazards: examples of ground water contamination, faults, cavities. *J. Appl. Geophys.*, 1995, **33**, 177–193.
26. Chlaib, H. K., Abdalnaby, W. and Abd, N., Application of the ground penetrating radar to detect weapons caches and unexploded ordnance: laboratory experiments. *IOSR J. Appl. Geol. Geophys.*, 2014, **2**, 41–50.
27. Polikar, R., The story of wavelets. In *Physics and Modern Topics in Mechanical and Electrical Engineering* (ed. Mastorakis, N.), World Scientific and Engineering Society Press, Greece, 1999, pp. 192–197.
28. Boggess, A. and Narcowich, F. J., *A First Course in Wavelets With Fourier Analysis*, Prentice-Hall, Englewood Cliffs, NJ, 2001.
29. Moreau, F., Gibert, D., Holschneider, M. and Saracco, G., Wavelet analysis of potential fields. *Inverse Problem*, 1997, **13**, 165–178.
30. Moreau, F., Gibert, D., Holschneider, M. and Saracco, G., Identification of sources of potential fields with the continuous wavelet transform: Basic theory. *J. Geophys. Res.*, 1999, **104**, 5003–5013.
31. Misiti, M., Misiti, Y., Oppenheim, G. and Poggi, J. M., *Wavelet Toolbox for Use with MATLAB User's Guide*, The Math Works Inc., Natick, MA, USA, 2000, p. 572.
32. Solla, M., Lorenzo, H., Rial, F. I. and Novo, A., Ground-penetrating radar for the structural evaluation of masonry bridges: Results and interpretational tools. *Construct. Build. Mat.*, 2012, **29**, 458–465.
33. Kofman, L., Ronen, A. and Frydman, S., Detection of model voids by identifying reverberation phenomena in GPR records. *J. Appl. Geophys.*, 2006, **59**, 284–299.

ACKNOWLEDGEMENTS. We thank NRSC, ISRO, Govt of India for funding project No. ISRO/RES/4/630/2016-17. We also thank UGC (UGC CAS, F560/1/CAS/2009/SAP-1) and DST (No. SR/FST/ESI-104/2010), Govt of India for research funding to the Dept of Applied Geophysics, IIT(ISM), Dhanbad. We also thank the Director, IIT(ISM), Dhanbad and the HOD, AGP, IIT(ISM) for their keen interest in this study.

Received 12 July 2019; accepted 17 December 2019

doi: 10.18520/cs/v118/i7/1104-1111